Global Decarbonisation Journal, ISSN: 3050-0230

Evaluation of operation control parameters of a residential solar organic Rankine cycle with effects of expander-generator coupling

Cagri KUTLU(1), Mehmet Tahir ERDINC(2), Amin EHTIWESH(3), Michele BOTTARELLI(4), Yuehong SU(5), Saffa RIFFAT(6)

(1) School of Built Environment, Engineering and Computing, Leeds Beckett University, Leeds LS2 8AG, UK, (2) Department of Architecture and Built Environment, Faculty of Engineering, University of Nottingham, NG7 2RD, UK, ; Department of Mechanical Engineering, Tarsus University, 33400, Mersin, Turkey (3) Department of Architecture and Built Environment, Faculty of Engineering, University of Nottingham, NG7 2RD, UK, (4) Department of Engineering, University of Ferrara, 44122, Ferrara, Italy, (5) Department of Architecture and Built Environment, Faculty of Engineering, University of Nottingham, NG7 2RD, UK, (6) Department of Architecture and Built Environment, Faculty of Engineering, University of Nottingham, NG7 2RD, UK

DOI: https://doi.org/10.17184/eac.9437

Abstract: Solar-powered organic Rankine cycles (s-ORCs) are promising technologies for converting solar radiation into electrical energy, offering a viable alternative to conventional photovoltaics. However, the intermittent nature of solar radiation presents operational challenges, as these systems cannot regulate their heat input and rely entirely on solar energy availability. This study investigates the transient performance of a small-scale s-ORC system without thermal energy storage, focusing on how operational parameters influence system behaviour under variable solar conditions. A simulation model is developed, integrating effectiveness–NTU-based heat exchanger models and a validated expander–generator coupling sub-model that accounts for real-world responses such as torque balance, rotational speed, and internal leakage. Key control parameters, including the flow rates of the refrigerant, cooling water, and thermal oil, are examined to assess their influence on overall performance. The results show that solar heat input is the dominant factor affecting system efficiency, followed by the cooling water flow rate, which has a more significant impact than thermal oil flow. Based on a one-day simulation, the expander's volumetric efficiency was found to average around 60% due to leakage losses, and the expander predominantly operated under off-design conditions. The generator efficiency varied between 49% and 58%, with lower rotational speeds resulting in better conversion efficiency.

Keywords: Solar ORC, Scroll expander, Transient response, Operation control

1 Introduction

The utilization of solar energy for power generation has primarily been implemented using concentrating solar collectors. However, the fluctuating nature of solar heat input introduces instability that cannot be inherently managed by the organic Rankine cycle (ORC) alone, thus requiring appropriate control strategies. Among the methods proposed in the literature are constant pressure and sliding pressure operation modes. In sliding pressure operation, the evaporating pressure is the main controlled parameter to maintain operation according to heat source [1], [2]. Control approaches typically adjust system outputs in response to variations in heat source temperature often influenced by thermal storage tank dynamics or solar input which in turn affects the evaporator pressure.

The influence of expander rotational speed on ORC performance has been also explored in several recent studies. Sun and Peng [3] conducted an experimental investigation of a small-scale ORC system where the expander was mechanically coupled to a generator resulting in equal expander and generator speeds. Although no active control of rotational speed was implemented, their results showed that variations in heat source temperature and working fluid flow rate significantly influenced the expander speed, which in turn affected power output and generator performance. They concluded that mismatch between the expander and generator rated speeds limited efficiency, highlighting the potential benefits of introducing active speed control. In contrast, Hsieh *et al.* [4] employed a scroll expander with stepwise adjustable rotational speed. Their study demonstrated that selecting appropriate fixed speeds based on heat input levels specifically 900, 1350, and 1800 rpm allowed for optimization of evaporator pressure and system stability, especially under low heat transfer rates. Also, they presented that lower expander speed at low heat input helped increase evaporation pressure and improve system stability. Fatigati *et al.* [5] presented a model-based approach where expander speed was not externally imposed but emerged from the dynamic torque balance between the expander and generator. Their validated simulation highlighted how torque-speed dynamics, including internal leakage and off-design conditions, influence system behaviour.

To implement effective control strategies, dynamic modelling of solar organic Rankine cycles (s-ORCs) is essential for understanding their transient behaviour and optimising performance. For example, Manenti *et al.* [6],[7] conducted numerical simulations using DYNSIM to model the start-up operations of the Archimede Concentrating Solar Plant in Sicily. Their work identified critical aspects of switching operations and optimised the plant's control strategy. The authors identified the critical aspects of switch on and switch off operations for solar plant and also mapped and optimised the plant's control strategy. A comparative study between the use of different types of solar collectors was modelled by El Hefni [8]. He performed a comparative study of different types of solar collectors, including parabolic trough collectors (PTCs), compound parabolic collectors (CPCs), and solar hybrid combined-cycle power plants, using the Thermo SysPro-Modelica tool for dynamic simulation.

Recent advancements in thermal energy storage (TES) integration have significantly enhanced the flexibility of ORC systems powered by intermittent heat sources. Da-

niarta *et al.* [9] presented a detailed review on TES applications in low and medium temperature ORC systems, covering various TES configurations and materials, including sensible and latent heat storage. Their findings underline the necessity of selecting suitable TES and expander strategies to address fluctuating heat sources such as solar or waste heat, especially in the 100–350 ° C range, where partial evaporation or inefficient cycle operation may occur. Guo *et al.* [10] proposed a cascade utilization approach using dual-tank thermal storage in a multi-energy complementary system combining a parabolic trough collector, TES, ORC, and absorption heat pump. Their thermodynamic modelling and multi-objective optimization demonstrated significant improvements in system stability and renewable energy penetration. However, the dynamic behaviour of the ORC expander under transient solar inputs was not modelled in detail. Furthermore, Baghaei *et al.* [11] introduced a novel solar-powered hybrid energy storage system utilizing phase change materials (PCMs) with high-fidelity CFD-based modelling. While their work provides a realistic simulation of latent TES behaviour in CSP systems, the dynamic coupling between the TES and expander components under real-time solar fluctuations remains underexplored. While systems such as solar ponds offer a cost-effective means of collecting and storing low-grade solar heat [12], they often require significant land area. Moreover, the relatively slow thermal response of TES-integrated systems may limit their suitability for small-scale or highly dynamic energy applications. In contrast, this study focuses on a compact solar-driven ORC system designed to operate without thermal energy storage, thereby relying entirely on real-time solar input. When it comes to using direct expansion systems, control becomes even more important to ensure safe and stable operation.

Although volumetric expanders are promising candidates for small-scale ORCs, studies on their off-design operation are relatively scarce and typically limited to scroll or single-stage screw expanders [13], [14]. For example, Ziviani *et al.* [15] specifically examined single-stage screw expanders for low-temperature solar ORC systems and others examined screw expanders in solar-driven ORCs, but primarily focused on design aspects rather than operational control [16], [17]. Collings *et al.* [18] experimentally analysed a small-scale ORC with a scroll-type expander under various heat source temperatures. While the system was coupled to a generator *via* a magnetic drive, without dynamic interaction between the expander and generator. A recent review study [19] provides a comprehensive overview of control strategies for organic Rankine cycle (ORC) systems integrated with TES and two-phase expansion technologies. The review highlights that the primary fluctuating parameters in such systems are the heat source temperature and the working fluid mass flow rate. Various control approaches are categorised based on their ability to regulate these variables and optimise overall cycle performance. Among these, proportional-integral-derivative (PID) control remains the most widely adopted strategy in ORC applications. In PID-controlled systems, the working fluid pump functions as the actuator to manage flow through the evaporator and maintain stability in the closed-loop cycle. The evaporator plays a pivotal role due to its sensitivity to intermittent and fluctuating thermal inputs. Furthermore, the study discusses future trends in ORC control, emphasising the potential of advanced methodologies such as machine learning (ML), artificial

intelligence (AI), and reinforcement learning (RL) to enhance operational flexibility and predictive control capabilities.

Despite these advances, few studies comprehensively address expander-generator coupling and system-level control in TES-free s-ORCs under real-time solar variation. There remains a need for simulation tools that (i) capture transient interactions among components (ii) inform control strategies under off-design conditions, and (iii) support operational safety. Therefore, this study develops a transient model of a solar ORC system that integrates a scroll expander-generator coupling mechanism. Unlike some previous studies that often neglect transient expander behaviour or assume constant isentropic efficiency, this model includes a semi-empirical expander model with leakage and torque dynamics, enabling realistic system predictions under fluctuating solar input. This offers a novel framework to investigate safe and efficient off-design operation in small-scale s-ORC systems.

2 System description

The system consists of a solar collector loop, an ORC block, and a cooling water loop. While validation of the complete s-ORC system under real experimental conditions is constrained by the complexity of physical setups and variable operating environments, the component models employed in this study have been previously validated [20], which involved detailed testing under realistic thermal and dynamic load conditions [21]. To ensure consistency and maintain the applicability of the validated model, the working fluid (R123), expander–generator configuration, and system's rated power were retained in the present simulation. Each component is modelled to capture its transient response. Thermal oil is used as the heat transfer medium in the collector loop, delivering energy to the evaporator where it vaporises the ORC working fluid. Both the evaporator and condenser are simulated using the effectiveness-NTU method. Once the heat exchanger geometries are fixed, their surface areas are held constant, and the system is assessed under off-design conditions to investigate transient behaviour and control performance.

The condenser is cooled by a cooling tower, allowing the effect of the cooling water flow rate on system performance to be examined. ORC operation is modelled with a variable-frequency control mechanism to adjust the refrigerant pump flow rate in response to variations in solar radiation, cooling water flow rate, thermal oil flow rate, and ambient temperature. This ensures that the expander inlet maintains a dry vapor state. A simple schematic of the system is provided in fig. 1. The refrigerant enters the pump as a saturated liquid (state 1), where its pressure is increased to the evaporator pressure (state 2). In the evaporator section, the high-pressure refrigerant is heated to its saturation temperature, initiating the evaporation process. Once the refrigerant has fully transitioned from the liquid phase to the vapor state, additional superheating is applied (state 3) to ensure safe expansion in the scroll expander. The high-pressure, superheated refrigerant then enters the expander, where it experiences a drop in pressure and temperature before exiting at state 4. The final main component, the condenser, removes heat from the refrigerant, allowing it to condense back into a saturated liquid.

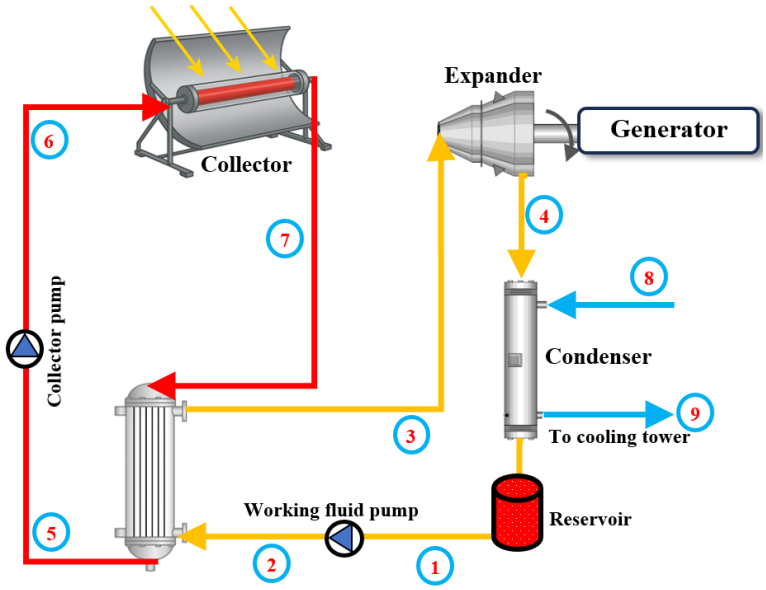

Figure 1: System schematic view of the system

2.1 Collector model

PTC-based power generation systems are the most mature and predominant systems among operational and under-construction plants [22]. Although PTC collectors need a tracking system and direct solar radiation to operate, their high thermal efficiency provide high temperature to run the ORC unit, thus, in this study PTCs are used in the simulations. Thermal collector efficiency is given as [23]:

$$\eta_{\mathrm{PTC}} = 0.762 - 0.2125 \cdot \frac{T - T_a}{G} - 0.001672 \cdot \frac{(T - T_a)^2}{G} \tag{1}$$

where T, T_a and G indicate collector inlet temperature, ambient temperature and beam radiation, respectively. Collected heat and collector outlet temperature can be calculated by Eq. (2):

$$\dot{Q}_{\mathrm{col}} = \eta_{\mathrm{PTC}} \cdot A_{\mathrm{PTC}} \cdot G = \dot{m}_{\mathrm{oil}} \cdot c_{p,oil} \cdot (T_{\mathrm{colout}} - T_{\mathrm{colin}}) \tag{2}$$

2.2 Evaporator and condenser model

The evaporator transfers the heat collected by the thermal oil to the working fluid. As the temperature of the thermal oil is expected to fluctuate over time due to variations in solar irradiance, the evaporator is modelled to respond dynamically to these temperature changes. To simplify the analysis and enhance practicality, pressure losses are neglected, and double-pipe heat exchangers are selected as the evaporator configuration in the solar ORC system.

As is well known, the working fluid is first preheated to its evaporation temperature, this section of the heat exchanger is referred to as the economiser. When the solar input varies, the evaporation pressure and, consequently, the saturation temperature and refrigerant mass flow rate also change. Since the heat transfer requirements depend on these parameters, the required heat exchange area must be recalculated under different operating conditions.

Although the total length of the heat exchanger is fixed, the lengths of the individual sections vary depending on operating conditions. Therefore, the system is designed such that the operating parameters are adjusted to ensure the refrigerant exits the evaporator in a superheated state. As shown in Figure 2, the evaporator consists of three sections with variable lengths, while maintaining a constant total length.

The effectiveness-NTU method was implemented by considering three sections in the evaporator. Details of the double pipe heat exchanger effectiveness-NTU method equations for single phase and two-phase flow can be found in the reference[24].

$$NTU = \frac{U \cdot A}{C_{\min}} \tag{3}$$

$$U = \frac{1}{\frac{1}{h_{\text{ref}}} + \frac{1}{h_{\text{oil}}}} \tag{4}$$

$$\varepsilon = \frac{1 - exp\left[-NTU \cdot (1 - C_r)\right]}{1 - C_r \cdot exp\left[-NTU \cdot (1 - C_r)\right]} \tag{5}$$

Where NTU is number of transfer units, U is overall heat transfer coefficient, ε indicates effectiveness, C_r is capacity ratio and h_{ref} and h_{oil} are heat transfer coefficients. Heat transfer coefficients can be determined as follows:

$$h = \frac{\text{Nu} \cdot k}{d} \tag{6}$$

Here, Nu, k and d represent the Nusselt number, the thermal conductivity of the refrigerant or thermal oil, and the tube diameter, respectively. To calculate the Nusselt number, an empirical correlation for pipe flow is employed. For each section of the heat exchanger, the effectiveness is calculated individually. Based on the corresponding heat transfer area requirements, the length of each section within the evaporator unit is determined. The condenser, which rejects heat from the refrigerant to the cooling fluid, is modelled in a similar manner. In the simulations, a cooling tower is employed as the cooling source. The condenser consists of two sections, and the same modelling approach used for the evaporator based on the effectiveness-NTU method and variable section lengths is applied to the condenser.

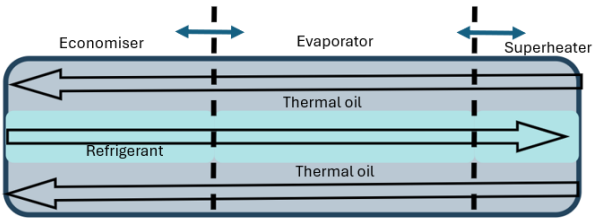

Figure 2: Double pipe heat exchanger diagram with three regions

2.3 Expander model

A scroll-type expander was selected for the simulation due to its compact design and widespread use in small-scale ORC applications. An improved semi-empirical model is employed to represent the scroll expander's performance accurately. [20]. By this model, not only shaft power can be found also electrical output can be calculated. Moreover, this model gives the rotational speed of the expander, in this way, refrigerant flow rate can be determined more accurately by considering flows in the pump and the expander.

The original scroll expander semi-empirical model was developed by Lemort *et al.* [25] it is the most preferable model recently. A schematic of the model is given in Figure 3 and as can be seen from the figure, many stages are included in the whole thermodynamic process.

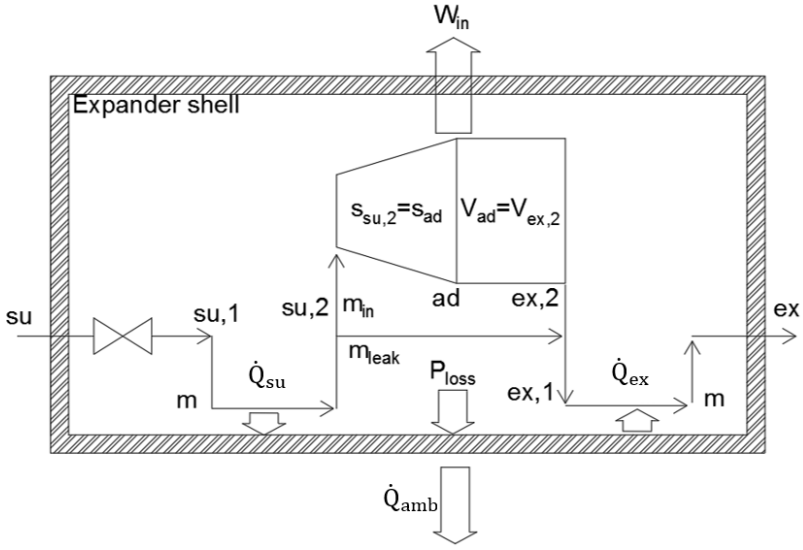

Figure 3: Semi empirical expander model adapted from the reference [25]

Lemort's model is composed of multiple theoretical stages.

1) Adiabatic pressure drops in supply side (su →su,1):

This stage represents the pressure drop occurring between the expander inlet and the suction chamber. The subscript su denotes the supply conditions. Cross sectional area A_{su} is considered for modelling isentropic flow through a nozzle.

$$\dot{m} = \rho_{su,1} A_{\mathrm{su}} \sqrt{2\left(h_{\mathrm{su}} - h_{su,1}\right)} \tag{7}$$

2) Isobaric supply cooling down (su,1→ su,2):

A heat transfer occurs between the fictitious envelope and refrigerant.

$$\dot{Q}_{\mathrm{su}} = \dot{m}\left(h_{su,1} - h_{su,2}\right) = \left[1 - e^{\frac{AU_{\mathrm{su}}}{\dot{m}c_p}}\right] \dot{m} c_p \left(T_{\mathrm{su}} - T_w\right) \tag{8}$$

$$AU_{\mathrm{su}} = AU_{su,nom} \left(\frac{\dot{m}}{\dot{m}_{\mathrm{nom}}}\right)^{0.8} \tag{9}$$

$U_{su,\,nom}$ is nominal supply heat transfer coefficient and T_w is wall temperature which is referred to expander shell temperature.

3) Internal leakage (su,2→ ex,2):

The entered mass flow is divided into two parts in the expander. Total mass flow is described as sum of the theoretical mass flow which depends on rotation speed, swept volume and inlet conditions, and leakage flow.

$$\dot{m} = \dot{m}_{\mathrm{th}} + \dot{m}_{\mathrm{leak}} \tag{10}$$

$$\dot{m}_{\mathrm{th}} = \rho_{su,2} V_{\mathrm{sw}} \frac{N}{60} \tag{11}$$

The leakage flow paths within the expander are modelled as a combined hypothetical area denoted by A_{leak}. This area is utilised in Eq. (12) to estimate the leakage flow, which is considered to follow an isentropic nozzle flow pattern.

$$\dot{m}_{\mathrm{leak}} = \rho_{\mathrm{leak}} A_{\mathrm{leak}} \sqrt{2\left(h_{su,2} - h_{\mathrm{leak}}\right)} \tag{12}$$

4) Adiabatic and reversible expansion to the adapted pressure (su,2 → ad):

Expansion of the volume depends on characteristics of the expander. Built in volume ratio defines the adapted volume of the expander.

$$v_{\mathrm{ad}} = BVR v_{su,2} \tag{13}$$

5) Adiabatic expansion at constant machine volume (ad → ex,2):

Under-expansion and over-expansion losses occur at this stage when the adapted pressure is either higher or lower than the system pressure at the expander outlet, respectively. To balance these pressures, the model assumes that fluid flows either into or out of the discharge chamber instantaneously when the expansion chamber connects to the discharge line. As is well-known, the performance of the expander is influenced by operating conditions and often involves off-design operation. Over-expansion occurs when the expander exhaust pressure exceeds the adapted pressure.

6) Adiabatic fluid mixing (ex,2 → ex,1):

Theoretical flow rate and leakage flow are adiabatically mixed, and mixture enthalpy is slightly increased.

$$\dot{m} \cdot h_{ex,1} = \dot{m}_{\mathrm{th}} \cdot h_{ex,2} + \dot{m}_{\mathrm{leak}} \cdot h_{\mathrm{leak}} \tag{14}$$

7) Isobaric exhaust cooling-down or heating-up (ex,1 → ex):

Heat transfer occurs between the fluid exiting the expansion chamber and the isothermal envelope, similar to the cooling process during isobaric supply. Once all the states are determined, the power generated by the expander can be calculated. The theoretical internal power of the expander is given by Eq. (15). To determine the actual shaft output power, mechanical losses are taken into account.

$$\dot{W}_{\mathrm{in}} = \dot{m}_{\mathrm{th}} \left[(h_{su,2} - h_{\mathrm{ad}}) + v_{\mathrm{ad}} \left(P_{\mathrm{ad}} - P_{ex,2} \right) \right] \tag{15}$$

Mechanical losses are lumped to mechanical loss torque; the equation is given;

$$\dot{W}_{\mathrm{sh}} = \dot{W}_{\mathrm{in}} - \frac{2\pi N \tau_{\mathrm{loss}}}{60} \tag{16}$$

Another heat transfer happened between the expander walls and ambient air.

$$\dot{Q}_{\mathrm{am}} = A U_{\mathrm{am}} \left(T_w - T_{\mathrm{amb}} \right) \tag{17}$$

Overall heat balance equation is given in Eq. (18). By solving overall heat balance equations, all variables can be found.

$$\dot{W}_{\mathrm{loss}} \pm \dot{Q}_{\mathrm{ex}} + \dot{Q}_{\mathrm{su}} - \dot{Q}_{\mathrm{am}} = 0 \tag{18}$$

The proposed model calculates the shaft power of the expander under various conditions. However, some equations include empirically determined parameters, such as A_{leak}, AU_{amb}, $AU_{su,n}$ and τ_{loss}. Since a different expander is used in this study, the required empirical parameters were derived using the expander's geometric model and experimentally obtained friction loss coefficients, as described in the reference paper [20].

To conduct the study, a MATLAB model was developed and iteratively solved. The simulation is based on several control schemes. As heat input cannot be constant because of the solar profile, a safe operation must be provided by control procedures. Control systems can be defined for component-based and system based. Collector-evaporator coupling reveals evaporation pressure, expander generator coupling determines the mass flow rate and expander outlet temperature, and finally, condenser-cooling tower coupling gives condensation pressure. Separately calculated parameters should be used for further iterations until reaching an acceptable convergence criterion. The procedure followed in the model is shown in Figure 4. The simulation begins by assuming the pressures at the pump inlet, evaporator inlet, and collector outlet temperature. The empirically determined refrigerant mass flow rate is then calculated as the initial step to determine the necessary parameters for the evaporator and expansion processes. With the evaporation pressure known, the inlet and exit enthalpies of the evaporator section are calculated, and the lengths of each section are determined based on the assumed parameters. If the required length exceeds the selected design length, the assumed evaporation pressure is updated, and the process is repeated. In the next step, the collector exit temperature is verified by calculations involving the solar heat input. If the assumed length cannot achieve the desired collector exit temperature, the values are updated, and the entire calculation is restarted. Once the heat exchanger and solar side are properly aligned, the expander model is executed.

The process begins by assuming the rotational speed, current, and expander wall temperature. Using these parameters and relevant equations, heat balance is applied. If the balance does not converge, the wall temperature is updated iteratively. Once the heat balance is satisfied, the torque balance for the expander-generator coupling is applied. The rotational speed and current are then updated, and the final electricity output is determined.

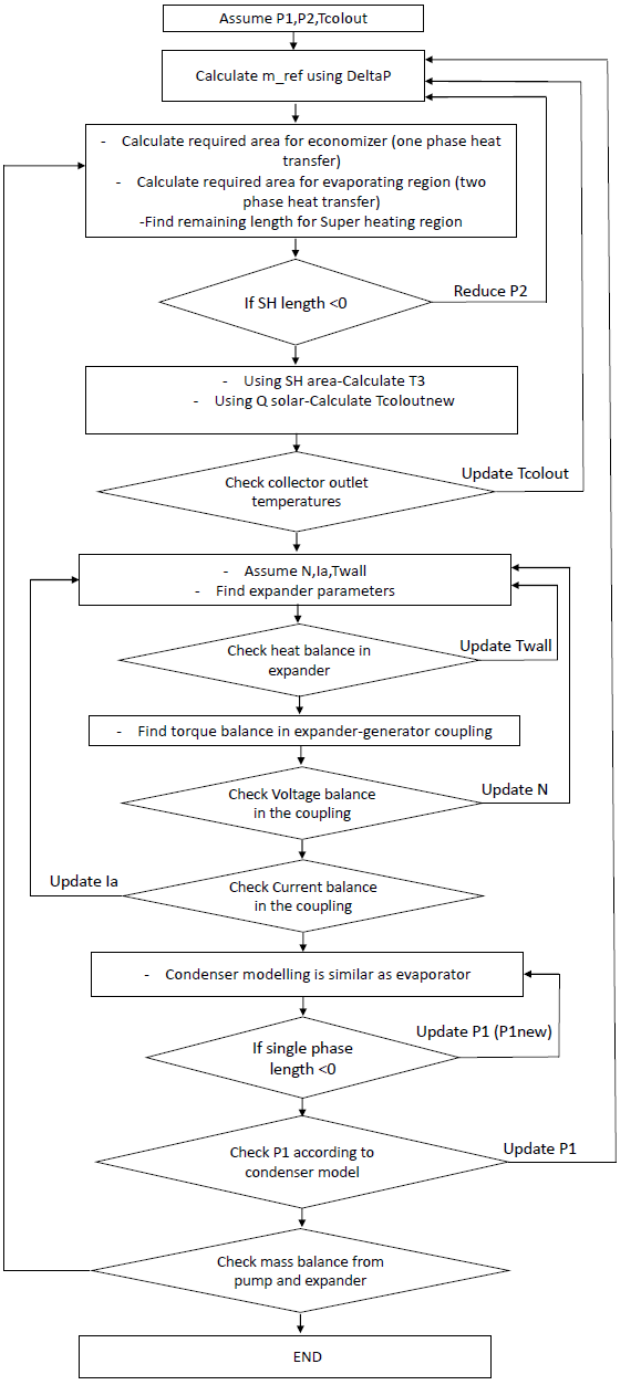

Figure 4: Flowchart of the procedure for predicting system outputs

3 Results and Discussions

The simulation model was developed in MATLAB. Initially, the effects of thermal oil and cooling water flow rates on system performance were evaluated under a design solar radiation level of 600 W/m². This was followed by an hourly transient simulation conducted over a full day. The remaining system specifications are presented in Table 1. Heat balances across both heat exchangers were assessed under all operating conditions to ensure energy conservation and consistency throughout the simulations.

Table 1. Design parameters

Collector area	13.2 m^2	Thermal oil flow rate	0.5 kg/s
Evaporator's total tube length	4 m	Cooling water flow rate	0.2 kg/s
Condenser's total tube length	4 m	Cooling water temperature	35 °C

3.1 Effect of thermal oil flow rate on performance

Thermal oil circulates through the solar loop, and the effect of its flow rate on the system's operation is presented. Figure 5 illustrates the calculated temperatures at different thermal oil flow rates. From the figure, it is evident that the flow rate of the thermal oil has minimal impact on the expander inlet and condenser outlet temperatures. This behaviour is primarily due to the type of solar collector used, which exhibits a high tolerance to changes in operating temperature, maintaining stable thermal efficiency over a broad range of conditions.

Specifically, the collector outlet temperature shows a noticeable decline as the thermal oil flow rate increases, indicating that higher flow rates enhance heat removal efficiency from the collector. However, despite the 20 K variation observed at the collector outlet, the evaporation pressure remains nearly unchanged. This is because the thermal efficiency of the collector only decreases by less than 1%, meaning that the overall heat input to the system remains relatively stable. Consequently, the system continues to operate under almost identical conditions, with no significant effect on key parameters such as the expander inlet and condenser outlet temperatures.

The stability in performance highlights the robustness of the system when using this type of solar collector. However, it should be noted that selecting a different type of collector could significantly influence system behaviour. For instance, collectors with lower thermal tolerance may experience larger efficiency drops, resulting in more pronounced variations in the evaporation pressure, expander inlet temperature, and overall system performance. This analysis also demonstrates that, under the current configuration, optimising the thermal oil flow rate primarily affects the collector outlet temperature, while the key performance indicators of the ORC system remain largely unaffected. Nonetheless, further studies could evaluate the impact of flow rates when using alternative collector technologies or when solar input varies significantly throughout the day.

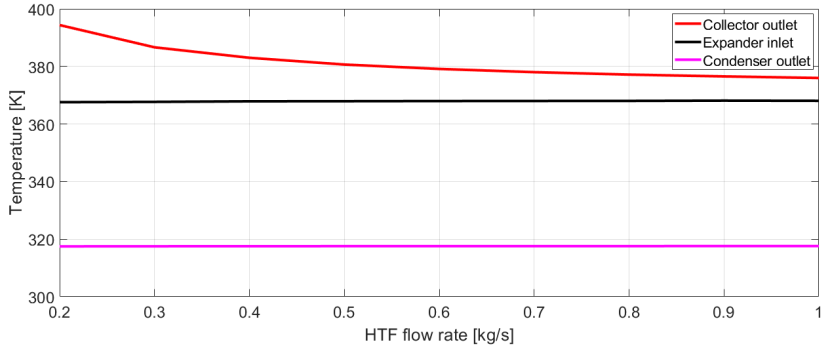

Figure 5: Effect of thermal oil flow rate on temperatures

3.2 Effect of cooling water flow rate on performance

To demonstrate the influence of the cooling water flow rate, Figure 6 illustrates the system's behaviour when a simplified expander model is used, assuming a constant isentropic efficiency and neglecting the effects of mass flow rate and electromechanical torque. As shown in the figure, increasing the cooling water flow rate from the cooling tower results in a decrease in condensing pressure. Meanwhile, the evaporation pressure remains nearly constant due to the steady solar irradiation. The increased pressure difference between the evaporator and condenser enhances the expander's capacity to perform mechanical work, leading to a higher shaft power output. Under design conditions, the increase in cooling water flow rate improves shaft power by approximately 30%.

However, to obtain more realistic system predictions, it is essential to incorporate the dynamic behaviour of the expander into the analysis. Figure 7 presents the impact of cooling water flow rate on system pressures and electricity output while accounting for the detailed expander model. Although the overall trend remains consistent with that shown in Figure 6, the pressure variations exhibit slight deviations. These differences can be attributed to the expander's regulation of the working fluid mass flow rate, which dynamically adjusts in response to changing operating conditions to maintain efficient performance. As expected, the electricity output is lower than the shaft power due to mechanical and electrical losses within the expander-generator assembly. Notably, Figure 7 reveals that the influence of the cooling water flow rate on system performance becomes more pronounced when expander dynamics are included, highlighting the importance of detailed component modelling in accurately capturing system behaviour.

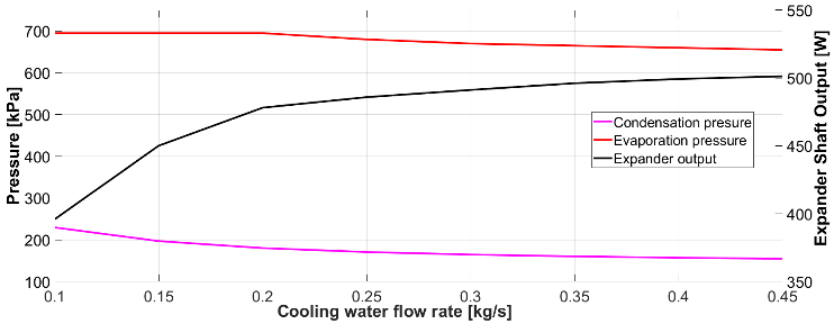

Figure 6: Effect of cooling water flow rate on operating pressures and expander work output for the solar irradiation of 600 W/m^2.

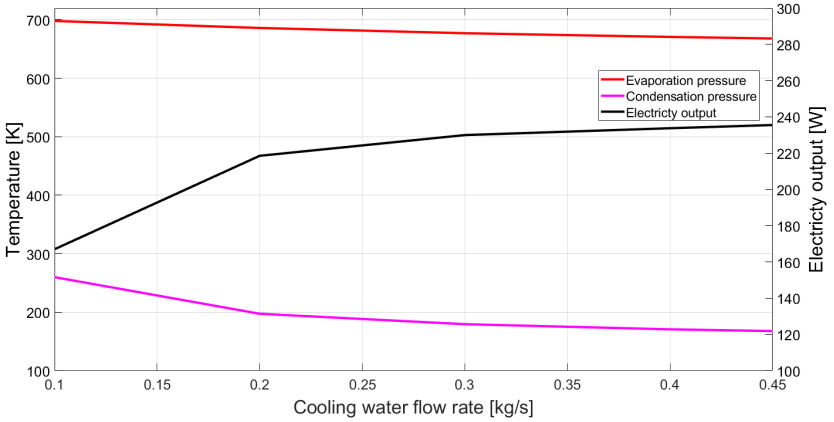

Figure 7: Effect of cooling water flow rate on operating pressures and electricity output for the solar irradiation of 600 W/m^2.

3.3 Daily performance of the solar ORC system

To evaluate the system's daily performance, simulations were conducted for a clear day with relatively high solar radiation. The solar irradiance varies between 300 and 900 W/m^2, while other parameters, such as the thermal oil flow rate, cooling water temperature, and flow rate, are held constant. Figures 8 and 9 show the variations in operating pressures, temperatures, and working fluid flow rates throughout the day.

As shown in Figure 8, an increase in solar irradiance leads to a steady rise in evaporation pressure due to the higher thermal input from the solar collector. This elevated heat input also causes an increase in the working fluid mass flow rate, as the system adjusts to maintain stable operation. However, during peak solar hours, the condensing pressure also rises. This behaviour can be attributed to the fixed cooling water flow rate, which becomes insufficient to dissipate the elevated heat load from the condenser effectively. Consequently, the condenser is unable to maintain a stable

condensing temperature, resulting in a gradual increase in both condensing pressure and temperature.

Figure 9 presents the temperature variations at key locations within the system throughout the day. The collector outlet temperature increases sharply in the morning as solar radiation intensifies, reaches its peak around midday, and gradually declines in the afternoon. A similar pattern is observed at the expander inlet, as its temperature closely follows that of the collector outlet due to the direct heat transfer between the two components. In contrast, the condenser outlet temperature exhibits only a slight increase over the course of the day. This limited variation highlights the constraints of maintaining a constant cooling water flow rate, which becomes less effective in managing the elevated thermal load during peak solar periods.

These results highlight the importance of adequate cooling capacity in maintaining optimal system performance. Insufficient cooling leads to elevated condensing pressures, which reduce the pressure differential across the expander and, consequently, diminish the system's power generation efficiency.

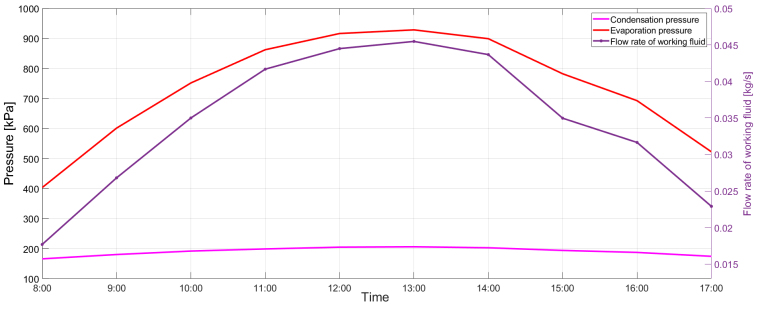

Figure 8: Variation of operating pressures, refrigerant flow rate and expander output. $\dot{m}_{\text{oil}}$=0.5 kg/s, $\dot{m}_{\text{water}}$=0.25 kg/s

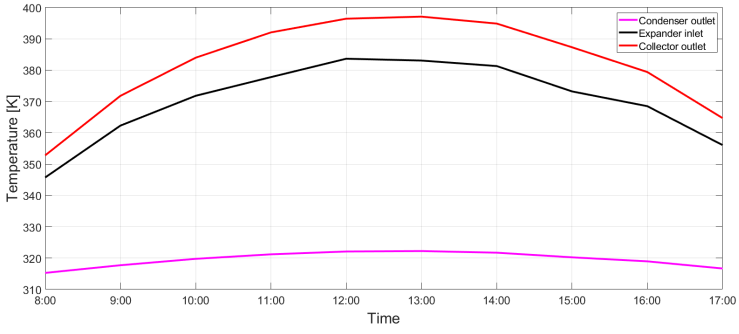

Figure 9: Variation of operating temperatures with time. $\dot{m}_{\text{oil}}$=0.5 kg/s, $\dot{m}_{\text{water}}$=0.25 kg/s

Figure 10 illustrates the variation in shaft power, electrical output, and expander rotational speed throughout the day. As expected, shaft power remains consistently higher than electrical output due to mechanical and electrical losses in the generator and coupling system. However, the conversion efficiency between mechanical and electrical power is not constant. While rotational speed increases during peak solar hours, the gap between shaft and electrical power also widens slightly, indicating a drop in electrical efficiency at higher speeds. This trend may be attributed to increased internal losses within the generator or suboptimal matching between the expander's output and the generator's design speed.

The results suggest that for much of the day, the system operates below the generator's rated speed, which presents an opportunity for optimisation. By externally adjusting parameters such as electrical load resistance, generator control strategy, or expander speed, it may be possible to better synchronise the mechanical input with the generator's optimal operating range. Moreover, the dynamic nature of solar radiation has a direct impact on rotational speed and, consequently, on power output and efficiency. During periods of high solar input—corresponding to peak shaft power and speed—the system shows increased output but slightly reduced efficiency. In contrast, during periods of lower irradiance, the reduced rotational speed aligns more closely with the generator's efficient operating range, resulting in relatively better conversion efficiency.

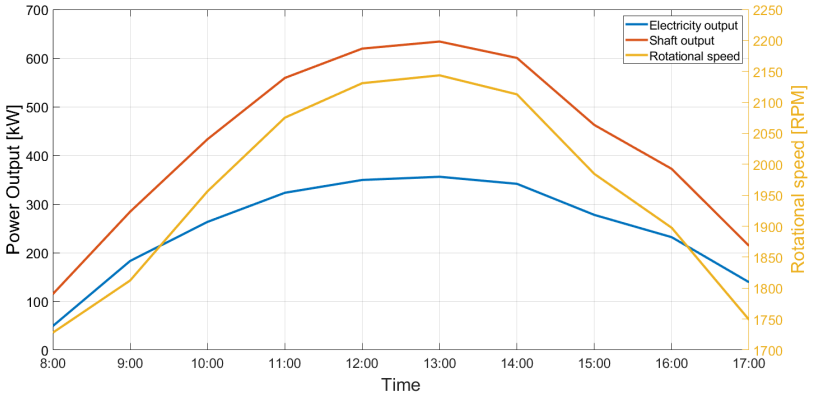

Figure 10: Variation of power outputs and rotational speed with time. $\dot{m}_{\text{oil}}$=0.5 kg/s, $\dot{m}_{\text{water}}$=0.25 kg/s

As shown in Figure 11, the expander's volumetric efficiency improves progressively from morning to afternoon. This trend is due to the decreasing relative impact of leakage as the total mass flow rate increases with rising solar input. In the early hours, leakage constitutes a significant proportion of the total flow, resulting in a lower volumetric efficiency (50%). However, during midday and early afternoon, efficiency rises to above 60% as the expander operates closer to its optimal range. This behaviour highlights the importance of minimising leakage and maintaining favourable pressure conditions to enhance expander performance, particularly during low-load periods.

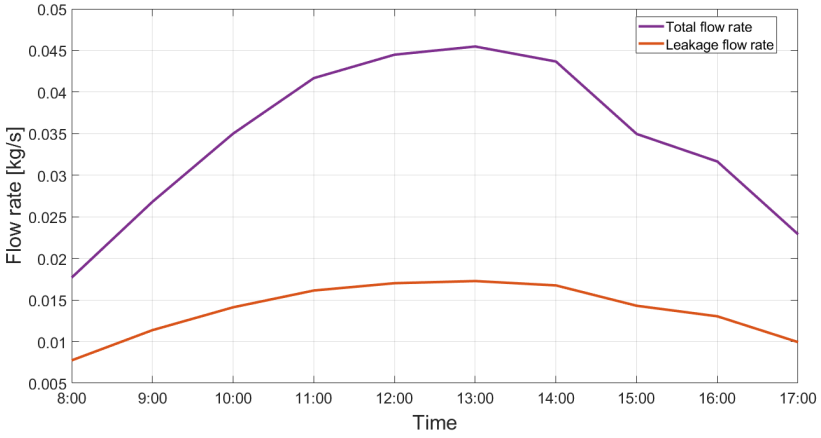

Figure 11: Variation of power mass flow rates through the expander. $\dot{m}_{\text{oil}}$=0.5 kg/s, $\dot{m}_{\text{water}}$=0.25 kg/s

4 Conclusions

In this study, a transient simulation model of a solar organic Rankine cycle system was developed, incorporating the dynamic thermal and mechanical responses of key components. The model included detailed heat exchanger representations using the effectiveness–NTU method, as well as a semi-empirical scroll expander model with expander-generator coupling and internal leakage losses. This approach allowed for a realistic evaluation of off-design operation and control strategies in storage-free solar ORC systems.

Controlling the refrigerant pump flow rate ensured that the working fluid entered the expander in a vapor state, enabling safe and stable system operation. Parametric analyses were conducted to evaluate the impact of thermal oil and cooling water flow rates under a reference solar radiation of 600 W/m², followed by a full-day transient simulation. The results revealed that solar heat input was the dominant factor influencing evaporation pressure and mass flow rate. However, among the two flow control parameters, cooling water flow rate had a greater effect on system performance compared to thermal oil flow rate.

- Specifically, increasing the cooling water flow rate resulted in a 30% increase in shaft power output under design conditions, primarily due to the reduced condensing pressure and higher pressure differential across the expander.

- The generator efficiency ranged from approximately 49% to 58% over the day, with higher efficiency observed during lower rotational speeds in the morning and afternoon.

- Volumetric efficiency of the expander varied between 50% and 64%, improving throughout the day as leakage became a smaller fraction of the total flow rate.

References

[1] J. Wang, Z. Yan, P. Zhao, and Y. Dai, "Off-design performance analysis of a solar-powered organic Rankine cycle," *Energy Convers Manag*, vol. 80, p. 150–157, 2014, doi: 10.1016/j.enconman.2014.01.032.

[2] C. Kutlu, J. Li, Y. Su, Y. Wang, G. Pei, and S. Riffat, "Investigation of an innovative PV/T-ORC system using amorphous silicon cells and evacuated flat plate solar collectors," *Energy*, vol. 203, p. 117873, 2020, doi: 10.1016/j.energy.2020.117873.

[3] J. Sun and B. Peng, "Experimental study on steady-state operation of organic Rankine cycle system under different operating conditions," *Sci Rep*, vol. 15, no. 1, Dec. 2025, doi: 10.1038/s41598-024-84813-2.

[4] J. C. Hsieh, Y. H. Chen, and Y. C. Hsieh, "Experimental study of an organic Rankine cycle with a variable-rotational-speed scroll expander at various heat source temperatures," *Energy*, vol. 270, May 2023, doi: 10.1016/j.energy.2023.126956.

[5] F. Fatigati, M. Di Bartolomeo, and R. Cipollone, "Model-based optimisation of solar-assisted ORC-based power unit for domestic micro-cogeneration," *Energy*, vol. 308, Nov. 2024, doi: 10.1016/j.energy.2024.132785.

[6] P. Vitte, F. Manenti, S. Pierucci, X. Joulia, and G. Buzzi-Ferraris, "Dynamic simulation of concentrating solar plants," *Chem Eng Trans*, vol. 29, p. 235–240, 2012, doi: 10.3303/CET1229040.

[7] F. Manenti and Z. Ravaghi-Ardebili, "Dynamic simulation of concentrating solar power plant and two-tanks direct thermal energy storage," *Energy*, vol. 55, p. 89–97, 2013, doi: 10.1016/j.energy.2013.02.001.

[8] B. El Hefni, "Dynamic modeling of concentrated solar power plants with the ThermoSysPro library (Parabolic Trough collectors, Fresnel reflector and Solar-Hybrid)," *Energy Procedia*, vol. 49, p. 1127–1137, 2013, doi: 10.1016/j.egypro.2014.03.122.

[9] S. Daniarta, M. Nemś, and P. Kolasiński, "A review on thermal energy storage applicable for low- and medium-temperature organic Rankine cycle," Sep. 01, 2023, *Elsevier Ltd.* doi: 10.1016/j.energy.2023.127931.

[10] Z. Guo, J. Wang, F. Dong, and H. Xu, "Multi-objective optimization of multi-energy complementary system based on cascade utilization of heat storage," *Energy Convers Manag*, vol. 299, Jan. 2024, doi: 10.1016/j.enconman.2023.117864.

[11] S. Baghaei Oskouei *et al.*, "Solar-powered hybrid energy storage system with phase change materials," *Energy Convers Manag*, vol. 302, Feb. 2024, doi: 10.1016/j.enconman.2024.118117.

[12] A. Saxena *et al.*, "A thermodynamic review on solar ponds," *Solar Energy*, vol. 242, p. 335–363, Aug. 2022, doi: 10.1016/j.solener.2022.07.016.

[13] G. Kosmadakis, D. Manolakos, and G. Papadakis, "Experimental investigation of a lowerature organic Rankine cycle (ORC) engine under variable heat input operating at both subcritical and supercritical conditions," *Appl Therm Eng*, vol. 92, p. 1–7, 2016, doi: 10.1016/j.applthermaleng.2015.09.082.

[14] R. Dickes, O. Dumont, R. Daccord, S. Quoilin, and V. Lemort, "Modelling of organic Rankine cycle power systems in off-design conditions : An experimentally-validated comparative study," *Energy*, vol. 123, p. 710–727, 2017, doi: 10.1016/j.energy.2017.01.130.

[15] D. Ziviani *et al.*, "Optimizing the performance of small-scale organic Rankine cycle that utilizes a single-screw expander," *Appl Energy*, vol. 189, p. 416–432, 2017, doi: 10.1016/j.apenergy.2016.12.070.

[16] M. Read, I. Smith, N. Stosic, and A. Kovacevic, "Comparison of organic rankine cycle systems under varying conditions using turbine and twin-screw expanders," *Energies (Basel)*, vol. 9, no. 8, 2016, doi: 10.3390/en9080614.

[17] K. Yang *et al.*, "Performance analysis of the vehicle diesel Engine-ORC combined system based on a screw expander," *Energies (Basel)*, vol. 7, no. 5, p. 3400–3419, 2014, doi: 10.3390/en7053400.

[18] P. Collings, A. McKeown, E. Wang, and Z. Yu, "Experimental investigation of a small-scale orc power plant using a positive displacement expander with and without a regenerator," *Energies (Basel)*, vol. 12, no. 8, Apr. 2019, doi: 10.3390/en12081452.

[19] A. R. Imre, S. Daniarta, P. Błasiak, and P. Kolasiński, "Design, Integration, and Control of Organic Rankine Cycles with Thermal Energy Storage and Two-Phase Expansion System Utilizing Intermittent and Fluctuating Heat Sources—A Review," Aug. 01, 2023, *Multidisciplinary Digital Publishing Institute (MDPI)*. doi: 10.3390/en16165948.

[20] C. Kutlu *et al.*, "Evaluate the validity of the empirical correlations of clearance and friction coefficients to improve a scroll expander semi-empirical model," *Energy*, vol. 202, p. 117723, 2020, doi: 10.1016/j.energy.2020.117723.

[21] J. Li, G. Gao, P. Li, G. Pei, H. Huang, and Y. Su, "Experimental study of organic Rankine cycle in the presence of non- condensable gases," *Energy*, vol. 142, p. 739–753, 2018, doi: 10.1016/j.energy.2017.10.054.

[22] J. Li, P. Li, G. Pei, J. Z. Alvi, and J. Ji, "Analysis of a novel solar electricity generation system using cascade Rankine cycle and steam screw expander," *Appl Energy*, vol. 165, p. 627–638, 2016, doi: 10.1016/j.apenergy.2015.12.087.

[23] A. Ehtiwesh, C. Kutlu, Y. Su, and S. Riffat, "Modelling and performance evaluation of a direct steam generation solar power system coupled with steam accumulator to meet electricity demands for a hospital under typical climate conditions in Libya," *Renew Energy*, vol. 206, p. 795–807, Apr. 2023, doi: 10.1016/j.renene.2023.02.075.

[24] C. Kutlu, M. Tahir, J. Li, Y. Wang, and Y. Su, "A study on heat storage sizing and fl ow control for a domestic scale solar-powered organic Rankine cycle-vapour compression refrigeration system," *Renew Energy*, vol. 143, p. 301–312, 2019, doi: 10.1016/j.renene.2019.05.017.

[25] V. Lemort, S. Quoilin, C. Cuevas, and J. Lebrun, "Testing and modeling a scroll expander integrated into an Organic Rankine Cycle," *Appl Therm Eng*, vol. 29, no. 14–15, p. 3094–3102, 2009, doi: 10.1016/j.applthermaleng.2009.04.013.